Imploded Shell Parameter Estimation Based on Radiograph Analysis

George Liu

Pittsford Sutherland High School

LLE Advisor: Reuben Epstein

Laboratory for Laser Energetics

University of Rochester

Summer High School Research Program

March 21, 2011

Abstract

High target density is an important condition for achieving ignition in direct-drive fusion experiments. High densities are momentarily created during a successful implosion. The OMEGA laser's 60 beams heat the target, causing the surface to ablate and compress the fusion fuel.[1] X-ray radiography is used to analyze the compressed target's optical thickness, which in turn describes the target's density. The higher the optical thickness, the darker the shadow cast. By recording the intensity of the backlighter x rays across the radiograph, the radiograph gives an attenuation profile. In a simple model of the shell, the changing attenuation across the radiograph depends on three parameters: inner radius, outer radius, and central radial optical thickness. A FORTRAN program was created to calculate the variances of the estimates of these three parameters in the presence of measurement error and a finite number of attenuation measurements limited by the finite resolution of the imaging device. Choosing the optimum optical thickness for the target by adjusting the backlighter photon energy minimizes the uncertainties of these estimates.

Introduction

The Laboratory for Laser Energetics uses two laser systems, OMEGA and OMEGA EP, to irradiate target capsules in inertial confinement fusion (ICF) experiments.[1] If the target reaches temperatures and densities high enough, it can achieve ignition, a condition during which fusion produces enough energy to sustain itself. The target does not always compress properly, however, due to imperfections in the spherical shell. To analyze and improve upon future direct-drive experiments, it is important to have diagnostics that can track the target capsule compression. X-ray radiography is one such diagnostic.

The density of the target can be measured indirectly by measuring the target's optical thickness τ, a description of the target's ability to absorb x-ray radiation. When the target absorbs x rays, a shadow is formed on the radiograph. By analyzing the shadow it is possible to estimate the optical thickness of the target. Estimation however always possesses some uncertainty. Measurement precision is limited, the x-ray framing camera has finite resolution, and other uncertainties may exist in the source of the backlighter, such as nonuniformity. For free-free radiography, the target's optical thickness varies with the photon energy of the penetrating x rays. This allows one to select the backlighter photon energy that provides the optimum shell optimal thickness, which creates a radiograph with a contrast profile that will allow the most precise model parameter estimates to be obtained. The central radial optical thickness τ_0, which is half the optical thickness of the imploded target viewed through its center, was chosen as the measure of the target's optical thickness. The value $\tau_0 = 0.5$ provides a unit central optical thickness that is the optimal value for a uniformly thick slab. To find the optimal optical thickness of a spherical capsule, whose optical thickness varies over the radiograph plane, a FORTRAN program was designed to calculate the parameter estimate uncertainties of a simple spherical shell capsule using covariance analysis based on hypothetical data. The dependence of the parameter estimate uncertainties on the central optical thickness was found and is shown below.

Parameter Estimation Uncertainty

The backlighter energy must be carefully selected to produce a useful radiograph. Information is lost if the backlighter produces too high or low an optical thickness. A high optical thickness (saturation) creates a dark shadow that allows only the outer edge of the shell to

be seen, while a low optical thickness (transparency) lets nearly all the x rays pass through, offering too low a contrast for the actual transmission contrast to be distinguished from the noise level σ_I. By modifying the target's optical thickness to produce shadows with distinct edges at both the inner and outer shell radii, it is possible to reduce the uncertainty in the parameter estimates.

The Radiograph Model and Optical Thickness

The radiograph model is a simplified representation of an imploded target shell and the x-ray intensity attenuation profile seen in its radiograph. Figure 1 shows a simple schematic of the radiography setup for a target shell that is assumed to be perfectly spherical and homogenous. Parallel x rays of intensity I_0 pass through the hollow target at various distances r from the capsule center and strike the radiograph plate with diminished intensity I. An actual radiography configuration of an experiment is more complicated because the target may not be uniform, homogenous, and spherical, and the backlighter rays selected by the imaging device may not be parallel. Nevertheless, this model provides a simple and relatively accurate representation that suffices for the purposes of this analysis.

The x-ray attenuation through the target is captured as the shadow on the radiograph and can be compared to the theoretical attenuation given by

$$I(r) = I_0 e^{-\tau(r)}, \tag{1.1}$$

where $\tau(r)$ is the optical thickness,[2] defined as the integral of the opacity κ, a function of spherical radius ρ, along the path s

$$\tau(r) = \int \kappa(\rho)\, ds\,. \tag{1.2}$$

Equation (1.1) ignores the effects of self-emission, the radiation emitted by the target, effectively assuming that the backlighter intensity I_0 is large in comparison to the self-emission. When the initial x-ray intensity I_0 and final intensity I are known, Eq. (1.1) can yield $\tau(r)$. The optical thickness can be calculated for every planar radial distance r to create an optical thickness profile $\tau(r)$. It is important to distinguish between the radii r and ρ in Eq. (1.2). The variable r is the radial coordinate in the plane of the radiograph, and ρ is the target-centered spherical radial coordinate at a point along the x-ray path. The variable r is planar while ρ is in 3-D space (see Fig. 1).

If the target's opacity is assumed to be uniform and if the x-ray path is assumed to be a straight line, Eq. (1.2) simplifies to the product of opacity and x-ray path length through the target:

$$\tau(r) = \kappa\, s(r)\,, \tag{1.3}$$

where s is the straight-line x-ray path length as a function of radius r in the image plane. The path length function can be expressed as three separate path length functions for three sections of the radiograph: where the x-ray travels through the shell and hollow, travels through the shell only, and misses the capsule entirely (see Fig. 1). Substituting the appropriate expressions for each condition of s yields the piece-wise function

$$\tau(r) = \begin{cases} 2\kappa\left(\sqrt{{R_2}^2 - r^2} - \sqrt{{R_1}^2 - r^2}\right) & \text{if } 0 < \mathrm{r} < R_1 \\ 2\kappa\left(\sqrt{{R_2}^2 - r^2}\right) & \text{if } R_1 < \mathrm{r} < R_2 \\ 0 & \text{if } \mathrm{r} > R_2 \end{cases}, \tag{1.4}$$

for a target capsule with inner radius $R_1$and outer radius R_2.

Methodology

Parameter estimate uncertainties were found using the weighted least-squares method. In this method, measurement errors are assumed to fall in a normal distribution, and the model, Eq. (1.4), is assumed to predict the correct values of $\tau(r)$ for the correct values of the parameters κ, R_2, and R_1. The most likely values of these parameters, based on a set of *N* measurements $I_{obs,i}$ at radius r_i with a random error σ_I, are those that minimize χ^2, the weighted sum of the measurement errors, which is given by

$$\chi^2 = \sum_{i=1}^{N} \frac{(I_{obs,i} - I(r_i))^2}{{\sigma_i}^2}, \tag{1.5}$$

where *i* is one of *N* measurements with random measurement error known as "variance" ${\sigma_i}^2$. The observed measurements $I_{obs,i}$ are readings from the experiment, and the predicted measurements $I(r_i)$ are the corresponding theoretical values obtained from the model.[3] For a model with *M* unknown parameters, collectively described as $\{x_j; j = 1, M\}$, the minimization of Eq. (1.5) is obtained when the partial derivative equations with respect to each parameter x_j equal zero:

$$\frac{\partial \chi^2}{\partial x_j} = 0\,. \tag{1.6}$$

The intensity model from Eq. (1.1), with τ replaced by its subcomponents given in Eq. (1.4), attempts to fit, using $M = 3$ parameters, κ, R_2, and R_1, an intensity model to a set of *N* intensity readings from a radiograph experiment with an uncertainty $\sigma_i = \sigma_I$ for each intensity measurement. The model has three partial derivative equations that must be set to zero to minimize χ^2:

$$\frac{\partial \chi^2}{\partial x_1} = \frac{\partial \chi^2}{\partial \kappa} = 0\,, \tag{1.7}$$

$$\frac{\partial \chi^2}{\partial x_2} = \frac{\partial \chi^2}{\partial R_2} = 0\,, \tag{1.8}$$

$$\frac{\partial \chi^2}{\partial x_3} = \frac{\partial \chi^2}{\partial R_1} = 0\,. \tag{1.9}$$

This set of equations can be written in matrix notation as

$$\sum_{i=1}^{M} \mathbf{J}\Delta\mathbf{x} = \mathbf{r}\,, \tag{1.10}$$

where the coefficient matrix **J** is a square matrix of length and width *M*, and $\Delta\mathbf{x}$ and **r** are both vectors of length *M*. The coefficient matrix **J** is given by

$$J_{jl} = \sum_{i=1}^{N} \frac{1}{{\sigma_I}^2} \frac{\partial I(r_i)}{\partial x_j} \frac{\partial I(r_i)}{\partial x_l}\,. \tag{1.11}$$

The residual vector **r** is found in a similar manner by

$$r_j = \sum_{i=1}^{N} \frac{1}{{\sigma_I}^2} \frac{\partial I(r_i)}{\partial x_j} \left(I_{obs,i} - I(r_i)\right)\,. \tag{1.12}$$

The residual vector **r** is multiplied with the inverse of **J** to produce the set of corrections $\Delta\mathrm{x_j}$ that, when added to the set of parameter estimates x_j, give a better set of parameter estimates. The improved parameter estimates are then used to calculate a new χ^2, and the process is repeated to find a new set of corrections. The process is iterated until the corrections become negligible, at which point χ^2 may be considered to have been minimized.

In planning an experiment in the absence of actual experimental measurements, the weighted least-squares method still provides formal estimates of the uncertainties of the parameter estimates.[3] It can be shown that the variances of the parameter estimates, ${\sigma_\kappa}^2$, ${\sigma_{R2}}^2$, and ${\sigma_{R1}}^2$, defined as the expected value of the squared difference between the parameter estimates

and their true values, are given by the diagonal elements of the inverse of the coefficient matrix **J**,

$$\sigma_i^2 = J^{-1}{}_{ii} . \tag{1.13}$$

This new matrix is referred to as the covariance matrix $\mathbf{J^{-1}}$. [3]

The covariance matrix yields the uncertainty of the parameter estimates as the variances σ_κ^2, σ_{R2}^2, and σ_{R1}^2, which describe the uniqueness of the model's fit to the data. The variances scale directly with the factor σ_I^2/N and roughly inversely with the square of the model's sensitivity to their respective parameters, as given by Eqs. (1.7) - (1.9) and suggested by Eq. (1.11).[3] Low uncertainty estimates indicated by small values of σ_{R1}, σ_{R2}, and σ_κ suggest that the parameter estimates can be accepted with greater confidence, while high uncertainty estimates suggest that the fit of the model to the data does not have a unique solution and that different sets of values of the parameters may fit the data comparably well. When σ_{R1}, σ_{R2}, and σ_κ are high, it is difficult to claim that the exact values of R_1, R_2, and κ have been estimated correctly.

Difficulties in Partial Differentiation

The weighted least-squares method relies extensively on partial derivatives of the intensity model to obtain **J** from Eq. (1.11). Due to the circularly symmetric nature of the radiograph data, it is not necessary to sum the partial derivative of every individual data point in assembling the coefficient matrix. Instead, a radial line of points from $r = 0$ to $r = R_2$ can give a close approximation for the summation by weighting each point to account for all other points of similar radial distance from the center. If each point is thought of as an arc segment, the circular radiograph can be partitioned into thin rings of width Δr such that any given ring will consist of a number of congruent segments given by

$$N_r = \frac{2\pi r}{\Delta r}, \tag{1.14}$$

where r is the ring's radial distance from the center, and N_r is the number of slices that "weights" the partial derivative of a single slice in the ring. The total number of measurements, N, is the sum of N_r over all the rings.

The finite-segment approximation of each data point also helps resolve conflicts in differentiation that arise when the radiograph readings are assumed to occupy an infinitesimal area. Taking the partial derivative of Eq. (1.1) with respect to each parameter yields

$$\frac{\partial I}{\partial \kappa} = -2(L_2 - L_1)e^{-2\kappa(L_2 - L_1)}I_0\,, \tag{1.15}$$

$$\frac{\partial I}{\partial R_2} = \frac{-2\kappa R_2}{L_2}e^{-2\kappa(L_2 - L_1)}I_0\,, \tag{1.16}$$

$$\frac{\partial I}{\partial R_1} = \frac{-2\kappa R_1}{L_1}e^{-2\kappa(L_2 - L_1)}I_0\,, \tag{1.17}$$

where

$$L_1 = \begin{cases} \sqrt{{R_1}^2 - r^2} & \text{if } 0 < \mathrm{r} < R_1 \\ 0 & \text{if } \mathrm{r} > R_1 \end{cases}, \tag{1.18}$$

$$L_2 = \begin{cases} \sqrt{{R_2}^2 - r^2} & \text{if } 0 < \mathrm{r} < R_2 \\ 0 & \text{if } \mathrm{r} > R_2 \end{cases}. \tag{1.19}$$

The partial derivatives given by Eq. (1.16) and Eq. (1.17) contain L_1 and L_2 in the denominator, which cause predicted partial derivative values near $r = R_1$ and $r = R_2$ to approach negative infinity. This is due to the piecewise nature of optical thickness in Eq. (1.4) which is embedded in the intensity model from Eq. (1.1) (see Figure 1). Trapezoidal approximations were used to estimate the partial derivatives at non-differentiable points.

The trapezoidal method assumes that the partial derivative of the intensity model changes at a constant rate across the width of a data point. The partial derivative can be approximated by averaging the partial derivatives of two neighboring points around the non-differentiable point. This method was used to calculate the partial derivative of Eq. (1.1) with respect to R_1 at $r = R_1$, where the partial derivative encounters a vertical asymptote. The approximation works because the data points are discrete with finite differences in their intensity values. By measuring the average partial derivative, one obtains a reliable estimate that may be used in Eq. (1.11).

Parameter Estimation from Radiograph Model

The FORTRAN program uses covariance analysis to calculate the uncertainty of the estimates of the three parameters R_1, R_2 and κ from the uncertainty of the hypothetical intensity measurements, which is equal to the intensity noise σ_I, and the spatial resolution, as expressed by the number of data points N. The variance calculation for each parameter was scaled to account for differences in resolutions and intensity variances of radiographs. The scaled variance multiplies the initial variance with the square root of N divided by the relative σ_I squared to divide out the effects of sample size and noise. The variance is also expressed as a ratio relative to the parameter estimate because the effects of uncertainty must be considered proportionally. Each is plotted against the central optical thickness τ_0, which was defined as $\tau_0 \equiv \frac{1}{2}\tau(0)$ to describe the path of travel along half the target diameter.

The graph of optical thickness variance in Fig. 2 shows a broad minimum near $\tau_0 \approx 0.5$ where the scaled optical thickness variance is minimized. The rapid increase of the variance as τ_0 increases or decreases suggests that departures from $\tau_0 \approx 0.5$ can result in significant degradation of the estimates. Even as the ratio of inner to outer radii changes, the minima of the

three plots remain approximately the same. The graph appears to support the initial proposed optimal central optical thickness of $\tau_0 \approx 0.5$ that applies to a uniformly thick slab.

The graphs of the scaled inner and outer radius variances in Fig. 3 show the same minimum near $\tau_0 \approx 0.5$ as seen in Fig. 2. The curves plotting the inner radius variance ("Radius 1 variance") have minima at slightly below $\tau_0 \approx 0.5$, and the graph of outer radius variance ("Radius 2 variance") continues to decrease past the minimum range, suggesting that departures above $\tau_0 \approx 0.5$ are safe for estimating the outer radius. This is because as the central optical thickness τ_0 increases, the outer shadow edge gets sharper. The graph of scaled opacity variance behavior in Fig. 4 is similar to the inner radius variance behavior, and further supports the optimal optical thickness calculation.

The graph in Fig. 5 shows the same results as Fig. 2 but with a linear vertical axis and logarithmic horizontal axis, showing more clearly the degradation when τ_0 is small and allowing it to be compared with comparable degradation at higher τ_0 values, where degradation due to saturation comes on rapidly. These results suggest that the degradation at lower optical thicknesses, $\tau_0 \lesssim 0.1$, such as in Compton radiography, may still be feasible in spite of the τ_0 value being off the optimum value, and that even stronger degradation is obtained with only modestly high optical thickness, $\tau_0 \gtrsim 1.0$. Fig. 2 offers less comparison between small and large τ_0 uncertainty estimates because the τ_0 scale is compressed at small τ_0.

Conclusion

Covariance analysis of hypothetical data with a simple, idealized model confirmed the optimum central radial optical thickness $\tau_0 \approx 0.5$ for the radiography of a perfectly spherical and homogenous imploded target in inertial confinement fusion experiments. The parameters

degrade rapidly as the target approaches saturation, with the exception of the outer radius R_2, and all of the parameters degrade as the target approaches transparency. The graphs obtained suggest the behavior of the parameter estimate degradation as τ_0 departs from the optimum. For example, estimation uncertainty is worse at $\tau_0 = 2.0$ than it is at $\tau_0 = 0.1$, which is surprising because the degradation at $\tau_0 = 2.0$, a relatively low saturation, is comparable to the degradation at $\tau_0 = 0.1$, a very weak signal. These results provide a better understanding of how radiography experiments may be tuned to produce better radiographs for parameter estimation.

Acknowledgments

I would like to thank Dr. Reuben Epstein for his time and support throughout the project. I would also like to thank Dr. Stephen Craxton for his encouragement and generosity for running the summer high school research program.

References

1. Lois H. Gresh, Robert L. McCrory, and John M. Soures. *Inertial Confinement Fusion: An Introduction*. Laboratory for Laser Energetics: Rochester, NY. 2009.
2. S. Chandrasekhar, *Radiative Transfer*, Dover Publications, New York, 1960; Reuben Epstein, "The Equation of Transfer," personal manuscript - private communication, 2010.
3. S. L. Meyer, *Data Analysis for Scientists and Engineers*, John Wiley & Sons, Inc., New York, 1975; Reuben Epstein, "Weighted Least-Squares Maximum-Likelihood Parameter Estimation," personal manuscript - private communication, 2010.

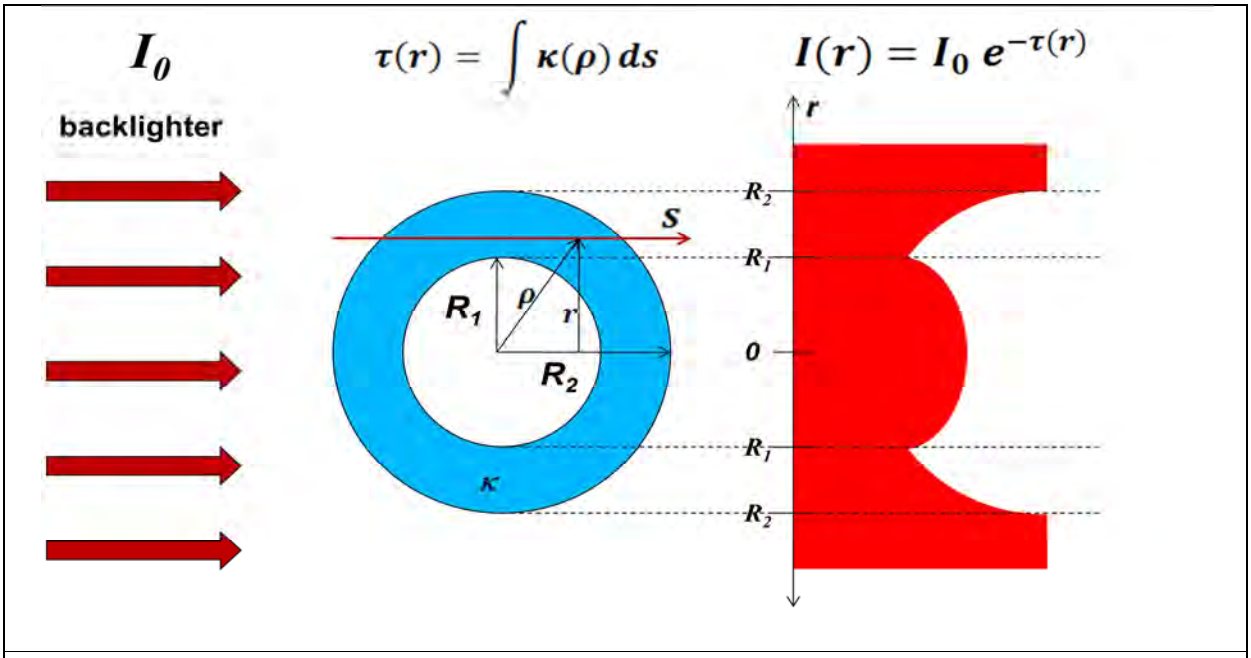

Fig. 1. A simple schematic of the radiography configuration in OMEGA. Parallel backlighter x rays of intensity I_0 pass through the hollow target at various distances r from the capsule radiograph center. The x-ray attenuation forms a "shadow" on the radiograph (shown on the right). For simplicity the target is assumed to be perfectly spherical and homogenous.

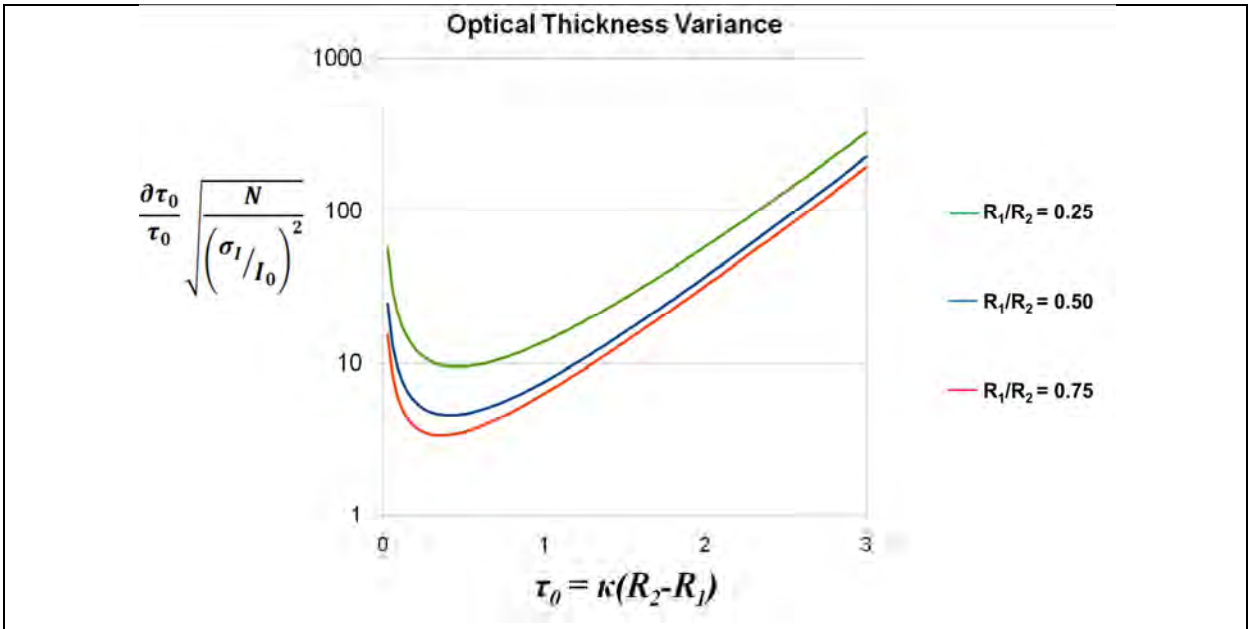

Fig. 2. A plot of the scaled relative optical thickness variance against central optical thickness. From top to bottom, the lines represent targets of inner radii R_1 = 0.25, 0.50, and 0.75. The vertical axis was scaled logarithmically to illustrate the broad minimum near $\tau_0 \approx 0.5$ for all three plots.

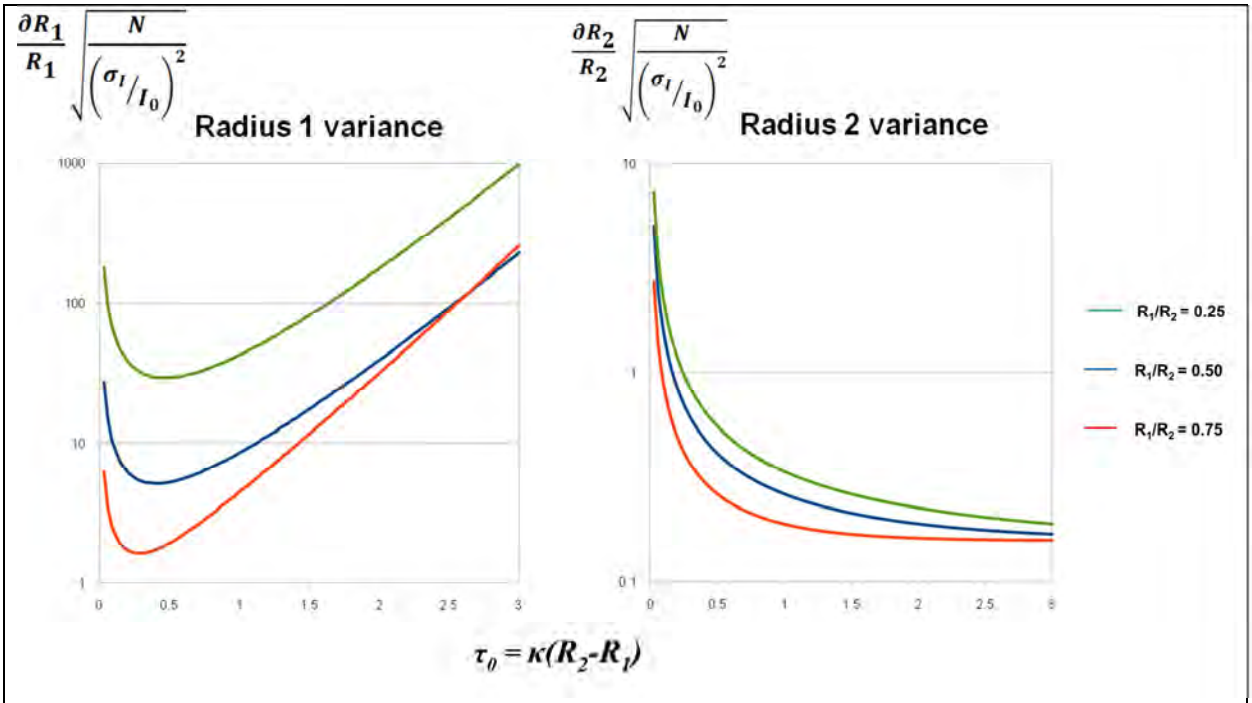

Fig. 3. Same conditions as in Figure 2. The scaled relative variances of R_1 and R_2 were plotted against the target's central optical thickness τ_0.

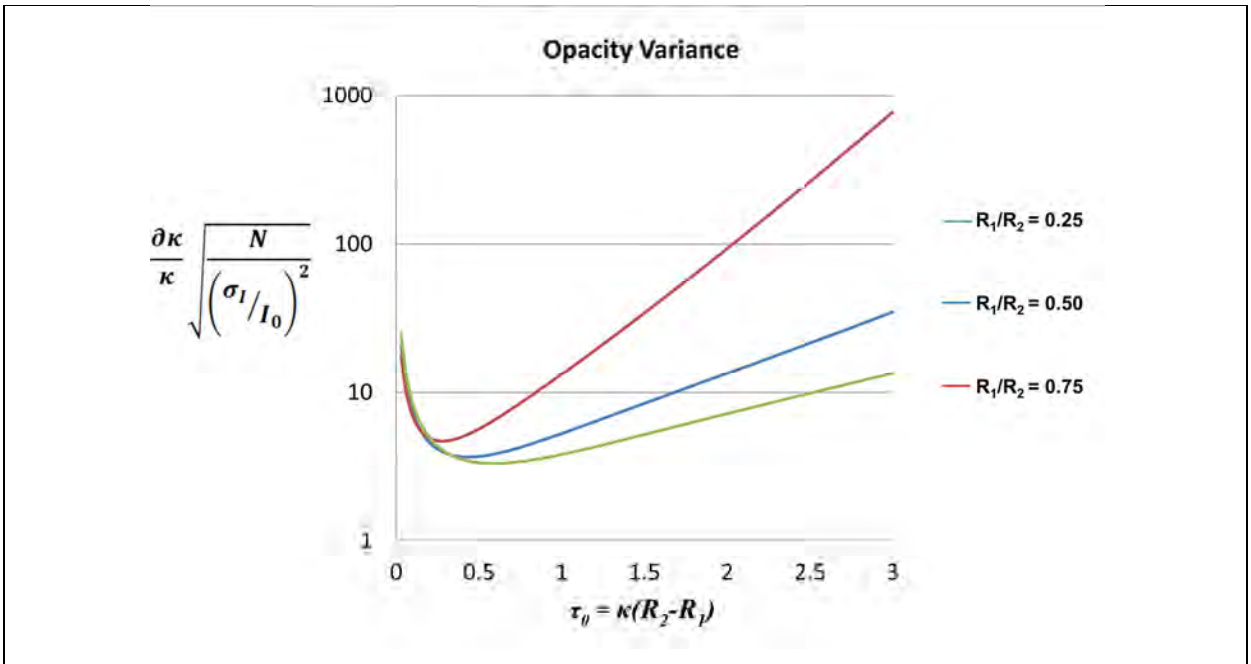

Fig. 4. Same conditions as in Figure 2. The scaled relative variance of opacity κ was plotted against the target's central optical thickness τ_0.

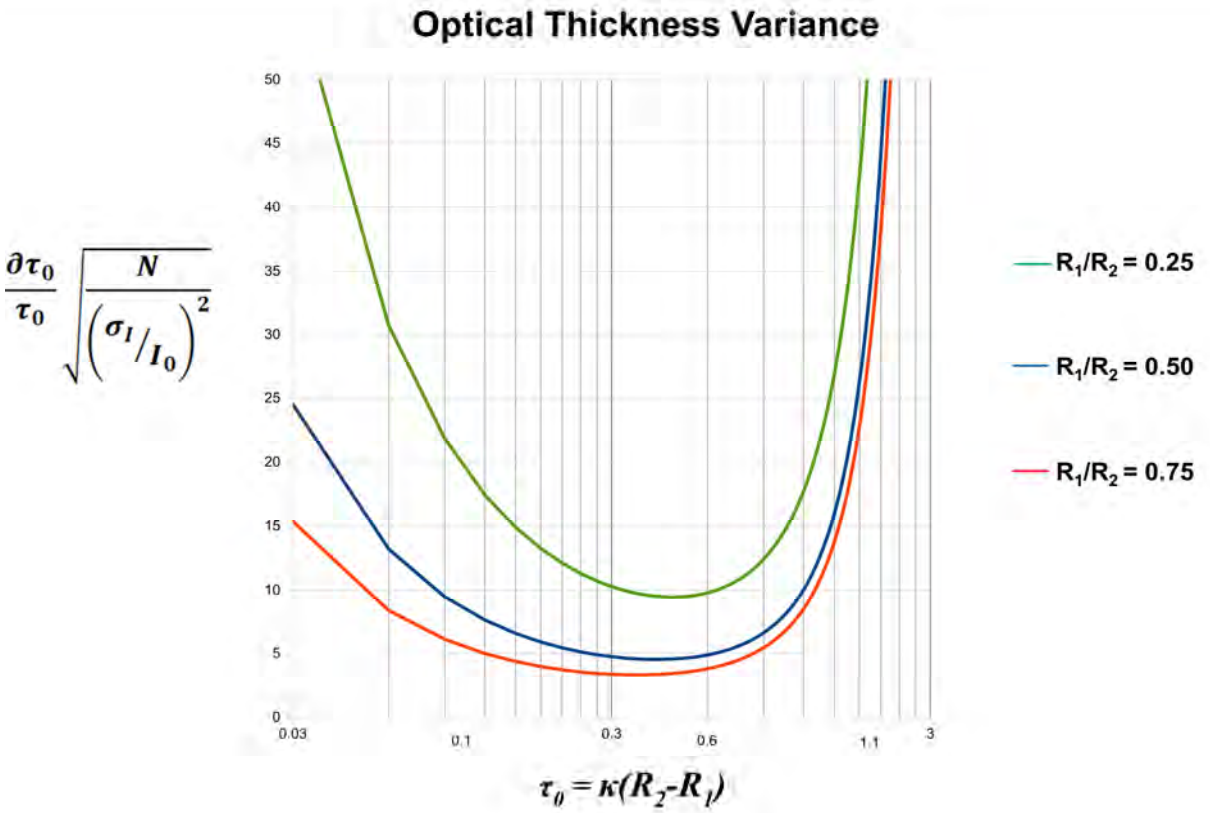

Fig. 5. Same graph from Figure 4 plotted on a logarithmic horizontal axis. The optical thickness estimate degrades rapidly as the central optical thickness τ_0 increases exponentially above τ_0 = 1.3. Notice the broad minimum near $\tau_0 \approx 0.5$.